JOURNAL OF MATERIALS SCIENCE **35** (2000) 4067–4072

Tensile rupture of tungsten alloys by the cascade of crack nucleation events

R. L. WOODWARD†
DSTO AMRL, PO Box 50, Ascot Vale 3032 Victoria, Australia

R. G. O'DONNELL
CSIRO Manufacturing Science and Technology, Private Bag 33, Clayton Sth MDC 3168, Australia
E-mail: odonnell@cmst.csiro.au

Quantitative metallographic methods are used to relate alloy ductility to microstructural fracture mechanisms for ten tungsten-nickel-iron alloys with Ni/Fe ratios of 7 : 3 and 1 : 1 and over the tungsten composition range 87.5 to 97.5 weight percent. These techniques are used to characterize the crack nucleation state at the rupture strain. The observations are consistent with fracture by load shedding and a cascade of nucleation events within a narrow zone in the sample. An instability analysis is presented which includes reduction in area due to both tensile plastic strain and to the development of crack nuclei within the sample.

1. Introduction

Whilst the strengths and ductilities of sintered tungsten-nickel-iron alloys are significantly influenced by composition and microstructure (size, shape and distribution of phases), these alloys also demonstrate widespread variations in mechanical properties which are often attributed to variations in interphase bond strength, and related manufacturing variables such as sintering conditions and initial powder purity [1–4]. In studying these alloys, the effects of these latter variables may be minimized by using alloys manufactured from the same powder source under the same conditions following established industrial procedures. In pursuit of high strengths and ductilities it is known that a high degree of tungsten grain contiguity should be avoided, the weakest fracture paths being provided by interfaces between tungsten grains [1, 2, 4]. The highest ductilities are achieved in alloys of 90 to 95 wt% tungsten and demonstrate a maximum in the percentage of transgranular cleavage of tungsten grains [2, 5]. Ductility is also influenced by the Ni/Fe ratio and by the presence of other minor element additions. In a comprehensive examination of composition effects and fracture paths, Ekbom [5] has pointed out that tungsten alloys are model two phase materials for the study of fracture and deformation, and similar observations have been made by Ostalaza Zamora *et al.* [6]. This present work builds on the results of earlier work [7] which examined the effect of composition on the properties of tungsten-nickel-iron alloys. This paper looks at microstructural influences on fracture path as a function of variations in parameters such as phase volume fractions, grain size and particle contiguity. The information is used to interpret fracture behaviour in relation to composition and microstructure.

2. Experimental

This study utilizes ten W-Ni-Fe alloys manufactured from the same source material in the same industrial plant so that manufacturing variables are minimized [7]. The tungsten contents are equally spread from 97.5 wt% to 87.5 wt% and two Ni/Fe ratios were used, namely 7 : 3 and 1 : 1. Details of the materials and their mechanical properties are given in the earlier work [7] and the strength and toughness data is summarised in Fig. 1. Changes in microstructure relating to these properties were determined by quantitative metallographic measurements using optical microscopy and electron probe micro-analysis.

Quantitative metallographic techniques [8] allow the measurement of grain size, estimations of tungsten grain surface area per unit volume, tungsten-tungsten contact area per unit volume, and tungsten grain contiguity (the fraction of tungsten surface area which is involved in particle-particle contacts). Binder (matrix) phase volume fraction was estimated using the quantitative capability of an electron probe microanalyser, considered to be more accurate than manual point counting. An examination of polished sections through the fracture surfaces of tensile test specimens in the electron microscope allowed the contributions of tungsten-tungsten (W-W) interface, tungsten-binder (W-B) interface, binder phase (B) and tungsten grain cleavage (W) fractures to be assessed. Measurements were made of the lineal proportion contributed by each fracture mechanism to the total 'length' of the sectioned fracture

† Deceased.

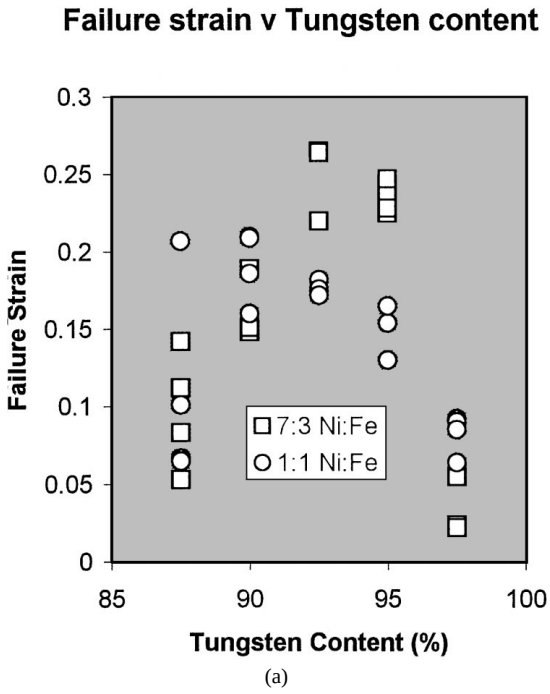

(a)

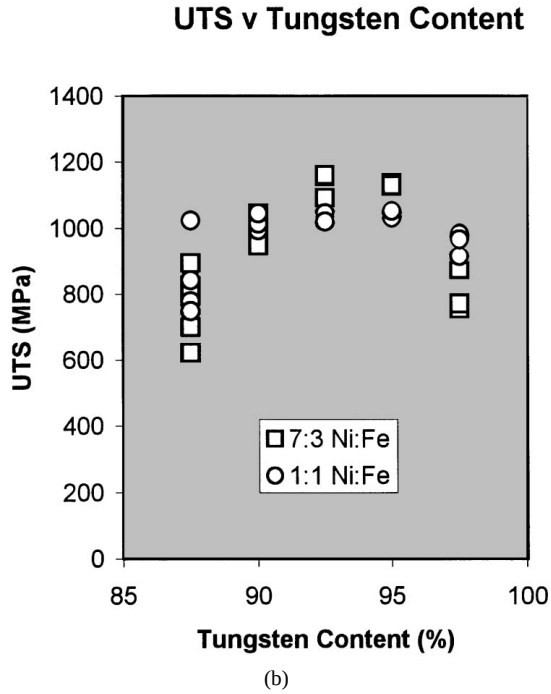

(b)

Figure 1 (a) Fracture strain as a function of tungsten content for the 7 : 3 and 1 : 1 Ni/Fe ratio alloys and, (b) true stress at the ultimate tensile strength as a function of tungsten content for the same alloys.

surface. From optical micrographs of sections through the body of the fractured tensile test specimens it was possible to determine the distribution of crack nuclei at the instant of rupture. For the four possible crack types, W-W, W-B, B and W, the cracked area per unit volume and the mean crack dimensions were measured within the body of these specimens at rupture.

3. Results

Table I lists the ten alloy compositions, with alloys identified 1 to 10 throughout this work, and gives a quantitative comparison of the microstructures. The grain size was similar in all alloys except for No. 10, with composition 87.5%W 6.25%Ni 6.25%Fe, which showed a smaller grain size. Alloy 5, 87.5%W 8.75%Ni 3.75%Fe, contained a small fraction of voids (∼0.05 volume fraction) which significantly influenced fracture behaviour and provided atypical results. The higher total tungsten surface area per unit volume and the slightly higher volume fraction of tungsten grains, in the 1 : 1 Ni/Fe alloys compared to the 7 : 3 ratio Ni/Fe alloys, are consistent with the binder phase containing 13.6 wt% W in the former case compared with 23.4 wt% W in the latter [7].

Table II presents measurements from the fracture surface of the contributions to fracture from each of the various fracture modes. It is noted that with the exception of the highest tungsten content alloys, where W-W interface fracture dominates, each of the four cracking mechanisms makes a significant contribution to the final fracture surface. Table III presents measurements from within the body of the specimens of the crack area per unit volume for each crack type. The total crack area per unit volume of all the cracks and their mean dimensions are also presented in Table III. In contrast to the results presented in Table II for the fracture surface, the observations in the body of the specimens (which can be taken as representative of the state of the specimen at the onset of rupture), show a domination of one fracture type, viz. tungsten-tungsten interface cracking.

4. Discussion

The 7 : 3 ratio Ni/Fe alloys show a peak ductility at about 92.5 wt% W, and this ductility is higher than the peak value for the 1 : 1 ratio Ni/Fe alloys, which occurs at about 90wt%W, as shown in Fig. 1a. Previous quantitative metallographic studies have generally correlated maxima in ductility with maxima in transgranular tungsten grain cleavage in such alloys; the low ductility at high tungsten contents corresponding to a higher proportion of tungsten-tungsten interface fracture, and the low ductility at low tungsten contents corresponding to high percentages of tungsten-binder pull-out and binder phase rupture. These observations are supported by measurements of the relative contributions to fracture surface area as presented in Table II, and these data are comparable to similar studies [5, 9] given the degree of subjectivity in these earlier measurements and the variability in material source and experimental conditions. The tungsten-tungsten grain contact area per unit volume and hence the contiguity, are generally higher in the 1 : 1 Ni/Fe alloys than in the 7 : 3 Ni/Fe alloys, Table I, and this is consistent with the 1 : 1 ratio alloys having generally lower ductilities if it is accepted that the tungsten-tungsten interfaces represent the lowest strength fracture mechanism.

An examination of the body of the fractured specimens, as quantified in Table III, presents an entirely different picture of fracture than that obtained by examination of the fracture surface alone. The maximum ductility for each Ni/Fe ratio correlates with a maximum in the total crack area per unit volume within the body, indicating greatest tolerance to the crack nuclei without crack propagation or crack linking. The

TABLE I Quantitative comparison of alloy microstructures

Alloy No.	W wt%	Ni wt%	Fe wt%	Grain size (μm)	W surface area per unit volume (mm^2/mm^3)	W-W grain contact area per unit volume (mm^2/mm^3)	Contiguity	Binder phase volume fraction
1	97.5	1.75	0.75	30	141	69	0.98	0.10
2	95	3.5	1.5	34	116	26	0.45	0.16
3	92.5	5.25	2.25	31	119	21	0.35	0.22
4	90	7	3	31	112	12	0.21	0.26
5	87.5	8.75	3.75	30	112	13	0.23	0.29
6	97.5	1.25	1.25	30	143	57	0.80	0.09
7	95	2.5	2.5	29	140	45	0.64	0.14
8	92.5	3.75	3.75	27	140	36	0.51	0.20
9	90	5	5	30	118	24	0.41	0.25
10	87.5	6.25	6.25	19	181	41	0.45	0.27

mean dimension for the cracks present in the body of the sample is about one third of the tungsten grain dimension. In all alloys the cracks are predominantly tungsten-tungsten interface cracks except for the one case where the percentage of pre-existing voids exceeded the cracking due to straining. This indicates that tungsten-tungsten interfaces are indeed the weakest link and that the contributions to fracture from other modes have developed during the final process of rupture. Cracked tungsten-tungsten interfaces within the body are generally oriented normally to the tensile axis. Most of the cracks involve separation at only one tungsten-tungsten interface, being stopped at either end by a tungsten grain or by the binder phase. Whilst these observations confirm that the tungsten-tungsten interface is the weakest crack path, a comparison of the cracked tungsten-tungsten interface area per unit volume in Table III with the total available tungsten-tungsten interface area per unit volume in Table I, shows that at the initiation of rupture only a small proportion of the available interface area is cracked. Rupture in the lower tungsten content alloys along a mixture of paths indicates that these other paths are not too much stronger than the tungsten-tungsten interface, as this shows it is easier to fracture by cleavage, tungsten-binder interface and binder phase fracture, than for the crack to branch slightly to seek other tungsten-tungsten interfaces. A similar conclusion was drawn in examining different fracture features in an investigation of sintering duration effects in a 95%W 3.5%Ni 1.5%Fe alloy [10].

Very few cracks were observed in alloy 10, 87.5%W 6.25%Ni 6.25%Fe, and, in this case only, they were not uniformly distributed but tended to be concentrated near the fracture surface. This too was the only alloy which showed necking prior to fracture in the tensile test. The cracks have therefore, in this case, appeared in the necked region where there is both increased stress and hydrostatic tension. A reduction in the interface area and hence 'flaw' size, between the smaller tungsten grains is believed responsible for the reduced cracking within this alloy.

To explain the link between the contribution of the fracture modes to the fracture surface, Table II, and the

TABLE II Percentage contributions of various crack paths to fracture

Alloy No.	W-W Interface	W-Binder interface	Binder Phase Rupture	Tungsten Grain Cleavage
1	100	0	0	0
2	26	47	3	24
3	33	14	13	40
4	12	47	23	18
5	28	37	29	6
6	89	6	4	1
7	53	27	10	10
8	39	11	11	39
9	21	34	18	27
10	10	36	26	28

TABLE III Fracture strain and measurements of cracking within fractured tensile test specimens

Alloy No.	Fracture Strain of sectioned sample	Crack Area Per Unit Volume (mm^2/mm^3) **[Mean Crack Width (μm)]**					
		Total All Cracks	W-W Interface	W-Binder Interphase	Binder Phase Rupture	Tungsten Cleavage	Pre-existing Voids
1	0.08	.16**[13]**	.16**[13]**	-	-	-	-
2	0.21	.98**[13.6]**	.92**[13.4]**	.07**[16.8]**	-	-	-
3	0.26	1.09**[13.3]**	.94**[12.7]**	.07**[15]**	.07**[35]**	.02**[8.2]**	-
4	0.18	.54**[26]**	.37**[33]**	.14**[18]**	.03**[21]**	-	-
5	0.13	.05**[14]**	.03**[15.2]**	.02**[12.6]**	-	-	.63**[35]**
6	0.09	.35**[11.6]**	.35**[11.6]**	-	-	-	-
7	0.15	.71**[11.9]**	.7**[11.9]**	-	-	.002**[4.8]**	-
8	0.17	.95**[12.3]**	.95**[12.3]**	-	-	-	-
9	0.21	3.02**[12.1]**	2.93**[12.4]**	.02**[8]**	.02**[11.4]**	.05**[7]**	-
10	0.19	.15**[5.6]**	.07**[5.6]**	.03**[5]**	.05**[6]**	-	-

TABLE IV True stress at UTS and parameters derived from quantitative metallographic data

Alloy No.	True Stress at UTS	Percentage of Cross Section Cracked*	Possible W-W Interface Fracture. Percentage of Total Cross Section	Stress Intensity Factor K (Eq 1) (MPa $\sqrt{m}$)
1	874	0.5	88	4.5
2	1133	3.3	37	5.9
3	1159	3.4	28	6.0
4	1053	1.7	15	7.6
5	895	0.2	17	4.7
6	973	1.1	72	4.7
7	1044	2.1	56	5.1
8	1029	2.5	41	5.1
9	1066	9.0	30	5.2
10	1026	0.1	33	(3.4)

development of cracking in the sample up to the point of rupture, Table III, it is necessary to consider the nature of the fracture process in terms of crack "path". If it is assumed that in rupturing the sample the crack is allowed to deviate by a maximum of one tungsten grain diameter (which is consistent with our experimental observations), then multiplying the crack area per unit volume, Table III, by the average tungsten grain diameter gives the proportion of the tensile test specimen which is cracked at the onset of sample rupture. These figures, presented in Table IV, show that this varies from less than 1% of the test specimen area for the alloys of low ductility to several percent for the more ductile alloys. The majority of the rupture process in these alloys is therefore a rapid catastrophic event associated with a small increment of strain and not a process of void growth and crack linkage as conventionally observed as the neck of a tensile sample develops with strain.

Multiplying one third of the tungsten-tungsten grain contact area per unit volume, Table I, by the average grain diameter, gives a measure of the proportion of the tungsten-tungsten interface that is correctly oriented to allow fracture along that path, with a crack deviation of not more than one tungsten grain diameter. These figures, presented in Table IV as the Possible W-W Interface Fracture, show that a very high proportion of tungsten-tungsten interface fracture is easily obtained in the high tungsten alloys and, apart from the 97.5wt%W alloys, is higher in the 1 : 1 Ni/Fe alloys compared to the 7 : 3 Ni/Fe alloys. Given the sampling errors in the quantitative metallography, the accord between these figures and the measured percentages of tungsten-tungsten interface fracture in Table II is reasonable, and it can be concluded that during the rupture process the vast majority of favourably oriented tungsten-tungsten interface areas are undergoing fracture.

The stress intensity level within the specimen associated with the crack nuclei, just prior to rupture, can be estimated based on a crack being considered as penny shaped in an infinite elastic medium [11]. This proposal suffers from the following limitations: there are multiple cracks present, even though they are fairly well separated; the figures for crack length used are average values from Table III, even though it may be presumed that the largest defect is the one which leads to final rupture; and the medium is not a homogeneous elastic continuum on the micro-scale being considered. Thus appreciable scatter in estimated stress intensity factor can be expected. Nevertheless a value for the stress intensity, K, was estimated from

$$K = \sigma\sqrt{(\pi a)} \tag{1}$$

Where σ is the tensile stress, and a is the half crack diameter.

The true stress at the ultimate tensile strength was used for calculations. This was also the stress at fracture except for alloy No. 10 which showed some necking. Despite the limitations in the analysis, the values of stress intensity factor listed in Table IV show only relatively small differences between the different alloys even though their final fracture modes vary significantly. This accords well with the suggested small differences in fracture strength for the different fracture paths. The absolute values of the calculated stress intensity factors are however approximately an order of magnitude less than the macroscopic toughness of the 95%W 3.5%Ni 1.5%Fe alloy as measured by Shah Khan, Underwood and Burch [12], namely 59.5 MPa·$m^{0.5}$, a figure consistent with values quoted for similar composition alloys [6]. The interpretation of these stress intensity figures is that, at the stress intensity calculated at the crack tips within the specimen the individual cracks do not propagate to cause rupture. As discussed above, with the exception of the single example of a low W content alloy (Alloy No 5), failure in these alloys was also not through a process of necking. Instead it is proposed that all these observations are consistent with rupture by a cascade of nucleation events within a narrow zone at the maximum load. It is necessary therefore to propose a process by which such an instability can occur and to assess the applicability of this process to the current alloys through quantitative means.

The different cracking modes will each have a distribution of strengths which overlap one another rather than having clearly distinct values, see Fig. 2. As the applied stress increases, cracking initiates with the lowest strength mechanism, W-W interface fracture, but before all such interfaces have cracked the weaker examples of the next mechanism begin to rupture, etc. It is confirmed from the mixture of fracture "paths" observed in these alloys that although the tungsten-tungsten interface is the weakest, the other mechanisms cannot be too much stronger as they are activated in preference to major crack branching to seek out only the weakest link. Whilst the total number of cracks within the sample just prior to rupture is small (representing between 0.1 and 9% of the total cross section for these alloys, Table IV) these cracks are expected to be increasing in number with strain. This cracking leads concurrently to load shedding about the crack sites as straining continues as well as a reduction of the load carrying area of the specimen. A reduced specimen cross section due to plastic strain in conjunction with the reduced effective cross section due to cracking,

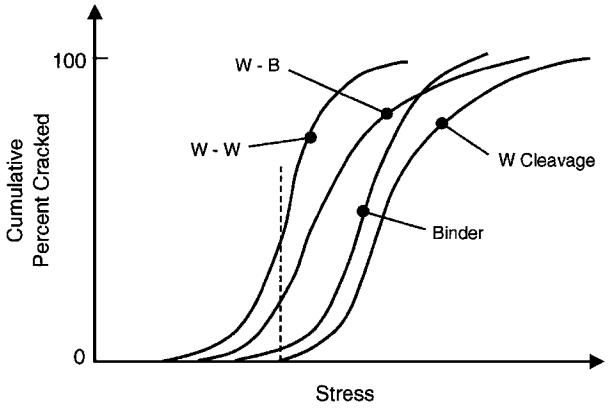

Figure 2 Schematic of the cumulative percentage cracked, of the four contributors to crack path, as a function of stress level. At the stress level indicated by the vertical line, individual contributions to total crack area in the material will come, in order, from W-W interfacial decohesion, W-B decohesion and binder phase rupture. The overall percentage of the cross section cracked will be a combination of those percentages cracked through each mechanism, and the percentage each mechanism contributes to the sample cross section.

and the load shedding associated with this, is believed to be responsible for initiating a cascade of individual fractures across one narrow section within the sample. During this cascade event, the fracture stress is readily exceeded at all possible fracture sites in that section. The process is shown schematically in Fig. 3.

Failure in a conventional tensile test may be predicted through a simple instability criterion. This can be extended to a material which undergoes internal cracking. For the conventional analysis of instability in tension, necking is predicted when the change in load carrying capacity due to the reduced cross-section exceeds the increased load carrying capacity due to increased sample strength through work hardening, or at instability

$$\frac{\mathrm{d}\sigma}{\sigma} = \frac{-\mathrm{d}A}{A} \tag{2}$$

where σ is the stess, and A is the area of the sample cross section.

In general where there is no internal cracking, the right hand side of Equation 2 is equivalent to the increment of strain, $\mathrm{d}\varepsilon$, and if the material stress/strain curve is expressed in terms of the equation

$$\sigma = \sigma_0 \varepsilon^n \tag{3}$$

where n, the work hardening exponent, and σ_0, are constants, then instability occurs at a strain equal to n [13]. To include the effect of internal cracking, all cracks of relevance are assumed to occur normal to the tensile axis, a fracture zone of width D is assumed, as in Fig. 3, and the crack area per unit volume is simply, for the present analysis, assumed to be proportional to strain, or

$$A_\mathrm{c} = C_1 \varepsilon \tag{4}$$

Where A_c is the area of cracking per unit volume, and C_1 is a constant for the material.

Whilst a threshold strain for crack nucleation and a more complex exponential or parabolic relationship with strain may be preferable, the linear relation of Equation 4 is appropriate in the light of the scarcity of data on cracking as a function of strain. The only data available for this work is the crack density at the point of rupture in Table III and this is a parameter rarely reported in the literature. Taking the density of cracks in the zone of width D, as well as the reduction in section due to straining into account, then the change in the load carrying area of the specimen with an increment of strain is given by

$$\frac{\mathrm{d}A}{A} = \mathrm{d}\varepsilon + DC_1\,\mathrm{d}\varepsilon \tag{5}$$

Combining Equations 2, 3 and 5 leads to an instability strain, ε_i given by

$$\varepsilon_\mathrm{i} = \frac{n}{(1 + DC_1)} \tag{6}$$

In this case the instability is due to an effective reduction in cross section by both plastic strain and cracking, so that load shedding and rupture may proceed by continued crack nucleation across that section. Values of C_1 can be obtained from Table III by dividing total crack area per unit volume by the rupture strain. D was assumed as equivalent to one tungsten grain diameter and n obtained by curve fitting the material stress/strain curves. Calculations using these parameters show that with this mechanism, rupture is possible in accord with Equation 6, at several percent strain less than the expected value for necking.

The proposed mechanism of a cascade of nucleation events accounts for the transition from the distribution of cracks in the bulk of the sample, as noted in Table III, to the utilisation of all available cracking sites on the fracture surface, Table II, with all of the weakest tungsten-tungsten interface fracture sites being used. In a sense the mechanism is one where a multitude of crack bridges are rapidly severed, however at the onset of the process there is more bridging than cracking for these alloys. The mechanism does not require propagation of individual crack nuclei, and sees "bridges" as a last step in linking the large number of nuclei which

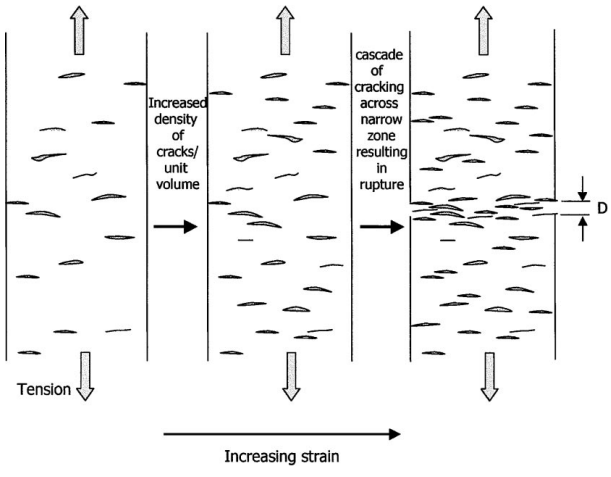

Figure 3 Schematic representation of the evolution of internal cracking with increasing strain and rupture by a cascade of crack nucleation events in a narrow zone of width D.

appear rapidly within the fracture zone with a small increment of strain. The mechanism is consistent with the observation of Rabin and German [9] that at high tungsten contents such alloys fail below the "uniform elongation" and with their conclusion that crack density increases with plastic deformation till a catastrophic crack propagation mechanism occurs.

5. Conclusion

Data are presented on tensile fracture strain and UTS as a function of composition for ten tungsten alloys. A wide range of microstructural parameters are measured using qualitative metallographic procedures and these are used to understand the nature of cracking for the different alloys. It is demonstrated that the tungsten-tungsten interface is the weakest link and primary nucleation site for fracture, but that rupture occurs by load shedding and a cascade of nucleation events utilising all available sites in the zone of fracture as the final step. A model is presented for the fracture process and this is shown to be consistent with an analysis for tensile instability based on reduction in area due to both plastic strain and cracking within the sample.

References

1. M. R. EISENMANN and R. M. GERMAN, *Int. J. Refract Hard Met.* **3** (1984) 86.
2. B. H. RABIN and R. M. GERMAN, *Met. Trans.* **19A** (1988) 1523.
3. B. H. RABIN, A. BOSE and R. M. GERMAN, in "Field Metallography, Failure Analysis and Metallography," edited by M. E. Blum, P. M. French, P. M. Middleton and G. V. Vandervoort (ASM International, Metals Park, Ohio, 1987) p. 285.
4. W. E. GURWELL, in Ann. Powder Metall. Conf. and Exhibition, Boston, MA, Metal Powder Industries Federation, May 1986, p. 1.
5. L. EKBOM, *Scandinavian Jnl of Met.* **20** (1991) 190.
6. K. M. OSTALAZA ZAMORA, J. GIL SEVILLANO and M. FUENTES PEREZ, *Mat. Sci. Eng.* **A157** (1992) 151.
7. R. G. O'DONNELL and R. L. WOODWARD, *Met. Trans.* **21A** (1990) 744.
8. U. UNDERWOOD, "Quantitative Stereology," Addison-Wesley, Reading, MA, 1970, p. 23.
9. B. H. RABIN and R. M. GERMAN, *Met. Trans.* **19A** (1988) 1523.
10. R. G. O'DONNELL, S. J. ALKEMADE and R. L WOODWARD, *J. Mat. Sci.* **27** (1992) 6490.
11. P. C. PARIS and G. C. SIH, ASTM STP No. 381, 1965, p. 30.
12. M. Z. SHAH KHAN, J. H. UNDERWOOD and I. A. BURCH in "Advances in Fracture Research," edited by K. Salama, K. Ravi-Chandar, D. M. R. Taplin and P. Rama Rao (Pergammon Press, March 1989) p. 1621. Proc. 7th Int Conf on Fracture (ICF7), Houston, Texas.
13. J. S. HOGGART, in "Fracture," edited by C. J. Osborn, R. C. Gifkins, J. S. Hoggart and D. S. Mansell (Butterworths, Australia, 1969) p. 15. Proceedings of the 2nd Tewksbury Symposium, University of Melbourne.

Received 6 August
and accepted 10 December 1999